



Atomistic Simulations of Hydrogen Effects on Lattice Defects in Alpha Iron

10

Shinya Taketomi and Ryosuke Matsumoto

Contents

1	Introduction	284
2	Hydrogen Trap Energy of the Trap Sites in Alpha Iron	286
2.1	Calculation of Hydrogen Trap Energy	286
2.2	Elastic Strain	287
2.3	Vacancies	287
2.4	Dislocations	288
2.5	Stacking Faults	288
2.6	Grain Boundaries	288
2.7	Free Surfaces	289
2.8	Hydrogen Trap Energy of Trap Sites in Alpha Iron	289
3	Hydrogen Effect on Individual Lattice Defects	290
3.1	Hydrogen Occupancy at Trap Sites	290
3.2	Hydrogen Effect on Vacancies	292
3.3	Hydrogen Effect on the Cohesive Energy of Grain Boundaries	293
3.4	Hydrogen Effect on Dislocation Mobility	293
3.5	Interaction Between Hydrogen and Individual Lattice Defects	294
4	Lattice Defects and Hydrogen Embrittlement Mechanisms	294
4.1	Interaction Between Many Lattice Defects	294
4.2	Cracks and Dislocations	294
4.3	Supersaturation of Vacancy Concentration Associated with Plastic Deformation ...	295
4.4	Reduced Lattice Defect Energy (Defactant-Like Effects)	296
5	Summary, Future Directions, and Remaining Problems	297
	References	298

S. Taketomi

Department of Mechanical Engineering, Saga University, Saga, Japan

e-mail: taketomi@me.saga-u.ac.jp

R. Matsumoto (✉)

Department of Mechanical Engineering and Science, Kyoto University, Kyoto, Japan

e-mail: matsumoto.ryosuke.6r@kyoto-u.ac.jp

© Springer Nature Singapore Pte Ltd. 2019

C.-H. Hsueh et al. (eds.), *Handbook of Mechanics of Materials*,

https://doi.org/10.1007/978-981-10-6884-3_11

283

Abstract

Solute hydrogen atoms degrade the strength of materials. This phenomenon, termed as hydrogen embrittlement (HE), has been a matter of concern for various industrial applications for more than a century. In recent years, HE has to be addressed because of the need for more efficient storage and transport of hydrogen. In this chapter, we present an overview of the current state of knowledge of the interaction between hydrogen and lattice defects. In Sect. 2, the hydrogen trap energy of various trap sites in alpha iron is reviewed and summarized. In Sect. 3, first, the hydrogen concentration around the defects is outlined based on the evaluation of the occupancy at each trap site. Subsequently, the effect of hydrogen on the stability and the kinetics of the lattice defects that trap hydrogen atoms are reviewed. In Sect. 4, mesoscopic calculations of the complex interactions among hydrogen-affected lattice defects are reviewed. Finally, the current state of knowledge of hydrogen effects on lattice defects and future directions are discussed. Alpha iron is considered because it is a basic steel component, and steel is a potential material for hydrogen storage and transport systems from engineering and economic viewpoints.

Keywords

Hydrogen embrittlement · Molecular dynamics · Density functional theory · Lattice defect · Mechanical property · Deformation

1 Introduction

It is well known that the strength of metals decreases in the presence of solute hydrogen [1–4]. This is known as hydrogen embrittlement (HE) and causes serious problems in the design and operation of various mechanical components. In recent years, hydrogen has attracted attention as a clean energy source. To use hydrogen as an energy source, we have to store and transport it. In addition, hydrogen is stored at a high-energy state (i.e., high-pressure gas or liquid state). Thereby, the chances of having failure of mechanical components owing to HE are high.

Although the mechanism of HE has been studied for more than a century, the overall embrittlement process has not yet been clarified even for simple material systems. Several embrittlement mechanisms for metals have been proposed. Hydrogen-enhanced decohesion (HEDE) [5, 6] is the earliest one and is based on the decrease of cohesive energy in the presence of hydrogen, i.e., cracks basically propagate in a brittle manner. Hydrogen-enhanced localized plasticity (HELP) [7–10] is another mechanism wherein hydrogen locally enhances the plastic deformation, i.e., the dislocation movement is enhanced at the crack vicinity. These two mechanisms have long been debated. Recently, M. Nagumo proposed the hydrogen-enhanced strain-induced vacancy (HESIV) mechanism [11, 12], in which hydrogen enhances the formation and coalescence of vacancies, resulting in

ductile fracture. R. Kirchheim also proposed the defactant concept [13] to describe the hydrogen stabilization of lattice defects. In any case, an understanding of the interaction between the solute hydrogen atoms and lattice defects is required to clarify HE.

The difficulty in understanding HE is attributed to the nature of the solute hydrogen atoms. Hydrogen atoms have high diffusivity within metals, and their distribution rapidly changes according to the distributions of the lattice defects and stress field. Hydrogen atoms also undergo complex interactions with the various lattice defects; thus, the direct evaluation by experiments of hydrogen distribution and its effect on lattice defects is extremely difficult. Thereby, atomistic and quantum-level simulations have been used to analyze the HE mechanisms. Several studies on the atomistic simulations of the effect of solute hydrogen atoms on the strength of materials have been published; however, none of them has quantitatively evaluated the hydrogen concentration under actual environmental conditions.

In this chapter, the hydrogen concentration near defects is evaluated. Subsequently, the effect of hydrogen on the stability and kinetics of individual lattice defects are reviewed. Next, the results of mesoscopic calculations of the complex interactions among hydrogen-affected lattice defects are reviewed. The subject material is alpha iron because alpha iron is a basic steel component and steel is a potential material for hydrogen storage and transport. The chapter comprises the following sections.

Section 2: The hydrogen trap energies of various trap sites, i.e., elastic strain field, vacancies, edge and screw dislocations, stacking faults, grain boundaries (GBs), and free surfaces, in alpha iron are reviewed. Then, the trap sites are ranked according to the magnitude of the trap energies. The obtained hydrogen trap energies in alpha iron are compared with those in aluminum.

Section 3: First, the hydrogen occupancy at each trap site under hydrogen gas conditions is obtained; then, the hydrogen effect on the stability and kinetics of each lattice defect is reviewed. It is evident that solute hydrogen affects the lattice defects; this is a function of the hydrogen concentration and deformation condition.

Section 4: Experimentally observed hydrogen embrittlement is the product of the interaction among lattice defects during deformation and fracturing. In this section, these phenomena and the competition among the various microscopic mechanisms are discussed based on large-scale molecular dynamics (MD) and discrete dislocation dynamics (DD) simulations, where the hydrogen effects on each individual lattice defect are modeled based on Sect. 3.

Section 5: The conclusions are summarized, and future directions as well as challenges are briefly discussed.

The relation among sections and subheads is shown in Fig. 1.

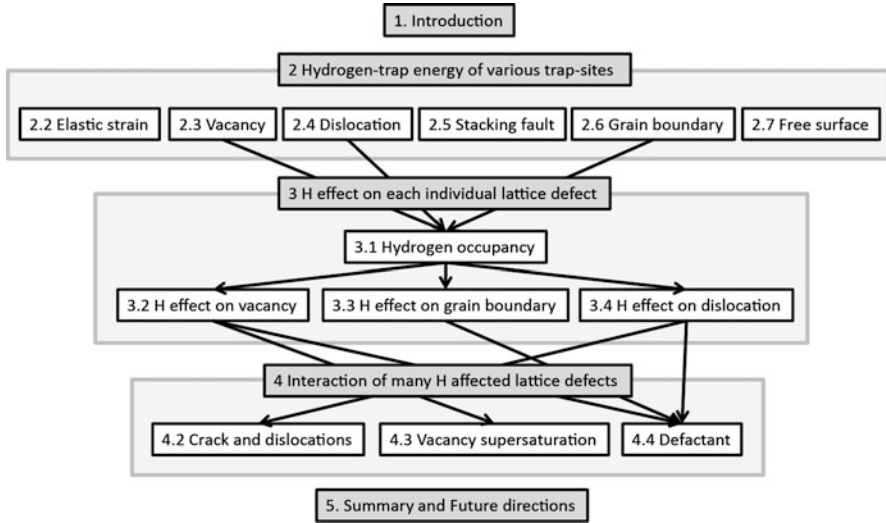


Fig. 1 Relations among sections and subheads

2 Hydrogen Trap Energy of the Trap Sites in Alpha Iron

2.1 Calculation of Hydrogen Trap Energy

Lattice defects are known to trap solute hydrogen atoms. Despite the progress in this matter, directly observing the hydrogen distribution in metals is still difficult because of the ultralow concentration of hydrogen atoms, their high diffusivity, and their small size and mass. This section reviews the interaction energy between solute hydrogen atoms and various trap sites obtained by atomistic and quantum-level simulations.

The binding energy between a solute hydrogen atom and a trap site is called hydrogen trap energy and is

$$E^{\text{Trap}} = E_{\text{HOS}} - \left(E_{\text{d+H}}(\mathbf{x}) - E_{\text{d}} - \frac{1}{2}E_{\text{H}_2} \right), \quad (1)$$

where E_{d} and $E_{\text{d+H}}(\mathbf{x})$ are the energy of the system before and after the introduction of a hydrogen atom at position \mathbf{x} , respectively, E_{H_2} is the energy of a hydrogen molecule, and E_{HOS} is the heat of solution into a material (0.27 eV; a hydrogen atom into a tetrahedral site (t-site) in alpha iron). For hydrogen atoms, considering the zero-point energy (ZPE) as a quantum effect owing to its small mass is crucial. The trap energies calculated via density functional theory (DFT) are all ZPE-corrected if no supplementary information is given. On the contrary, the trap energies calculated using interatomic potentials are not ZPE-corrected because the reference physical

properties used to develop the interatomic potential include ZPE. The details of the calculation procedure of the hydrogen trap energy using DFT and interatomic potentials have been previously determined [14–16].

2.2 Elastic Strain

It is generally believed that hydrogen atoms accumulate in high hydrostatic stress regions, such as ahead of mode-I crack tips and the tensile side around an edge dislocation. Several previous studies have included the hydrostatic stress gradient in the hydrogen diffusion equation as a hydrogen accumulation term [17–20]. This procedure well predicts the hydrogen diffusion in fcc and hcp metals. However, it has long been known that interstitial atoms that occupy octahedral sites (o-site) in the bcc lattice, such as carbon atoms in alpha iron, strongly interact with shear deformations [21, 22]. The hydrogen trap energy owing to both volumetric and shear strain was evaluated using the Vienna ab initio simulation package (VASP) [23–25] in Ref. [15]; shear strain (≈ 0.01) along a specific direction changes the most stable occupation site of a solute hydrogen atom from t-site to o-site. Furthermore, it was shown that despite that the trap energy arising from volumetric strain $\varepsilon_v = 0.05$, which is almost equal to the elastic strain around a dislocation core ($r > 0.5$ nm), is 0.154 eV, the shear strain yields maximum of ~ 0.2 eV depending on the direction.

Although the energy difference between sites is only 0.03 eV for undeformed lattices, the difference increases under shear strain, e.g., ~ 0.42 eV when the shear strain is -0.05 and ~ 0.1 eV when -0.01 [15]. Thus, elastic strain makes the potential surface of hydrogen diffusion uneven, and the diffusion coefficient and diffusion pass are significantly affected by shear strain, as directly confirmed near the core of edge dislocations by MD simulations [16].

2.3 Vacancies

Vacancies in alpha iron produce trap sites with extremely strong trap energy and attract multiple hydrogen atoms at nearby sites under hydrogen gas conditions, as shown in Sect. 3.1. Thus, calculating the hydrogen trap energy by sequentially introducing hydrogen atoms based on a stable order is essential. Tateyama et al. first performed extensive analyses of the hydrogen and (mono) vacancy interaction using DFT calculations and reported the hydrogen trap energy for up to six hydrogen atoms (0.56–0.04 eV) [26]. Furthermore, they showed that two hydrogen atoms are trapped at opposing o-sites in a vacancy and the hydrogen-vacancy complex (VH_2) forms planar or linear structures. In Ref. [27], using VASP [23–25], the following values are reported for the first to sixth hydrogen atom trapped at o-sites in vacancies: 0.64, 0.66, 0.34, 0.30, 0.21, and -0.16 eV. These values are in good agreement with the calculations [26] and experiments (0.63 and 0.43 eV) [28].

2.4 Dislocations

Dislocations are known to interact with the solute hydrogen atoms. Especially, elastic theory suggests that edge dislocations strongly interact with hydrogen atoms responding to the hydrostatic stress field, which is known as the Cottrell atmosphere. Dislocations are believed to keep moving in the Cottrell atmosphere, and this could be one of the hydrogen transport mechanisms within a metal. Thus, the interaction between solute hydrogen atoms and dislocations could play an important role in HE, i.e., plastic deformation and hydrogen transport. On the contrary, the development of computational resources and analytical techniques has contributed to the investigation of the interactions between dislocations and hydrogen. Atomic-scale investigations directly evaluate the effect of the dislocation core on the hydrogen trap and have suggested that the core structure could be the strongest hydrogen trap site [29]. In alpha iron, the major slip planes are $\{110\}$ and $\{112\}$, and the slip direction is $\langle 111 \rangle$ for both. Taketomi et al. calculated the hydrogen trap energy of typical trap sites within the core structure for $\{110\} \langle 111 \rangle$ and $\{112\} \langle 111 \rangle$ edge dislocations [30] using molecular statics calculations based on the embedded atom method developed by Wen et al. [31]. The maximum values are the same for both core structures, i.e., 0.49 eV; however, the distribution of trap sites differs. The detailed distribution of hydrogen trap energies around the $\{112\} \langle 111 \rangle$ edge dislocation is also given by Taketomi et al. [16]. The trap energy distribution around the core structure, i.e., the elastic strain field, is striped owing to the effect of shear strain on the bcc structure (see Sect. 2.2). These characteristics yield planar hydrogen diffusion in MD calculations. Conversely, the hydrogen trap energy for the screw dislocation core is estimated at 0.26 eV by first-principles calculations [32] and ~ 0.30 eV by the path-integral MD method [33].

2.5 Stacking Faults

It has been reported that hydrogen reduces the stacking fault energy, thereby increasing the width of the dislocation cores. Seki et al. evaluated the hydrogen trap energy at stacking faults and reported the hydrogen trap energies in $\{110\} \langle 111 \rangle$ and $\{112\} \langle 111 \rangle$ systems: 0.12 and 0.02 eV, respectively [14]. The interaction energy between hydrogen and stacking faults is extremely weak; thus, it is considered that hydrogen does not accumulate at stacking faults and the width of the dislocation core structure in alpha iron does not change except in extreme cases, i.e., very high hydrogen concentration.

2.6 Grain Boundaries

Riku et al. [34] estimated the hydrogen trap energy of GBs for $\langle 110 \rangle$ symmetrical tilt GBs (STGBs) and $\langle 001 \rangle$ twist GBs in alpha iron using atomistic simulations

with a similar procedure as that in Ref. [16]. They showed that the GB energy and hydrogen trap energies show good correlation, because high-energy GBs tend to have large gaps (free volume) and hydrogen atoms are more stable in the large gaps. This tendency was also confirmed using DFT calculations for two $\langle 110 \rangle$ symmetric tilt GBs: high-energy $\Sigma 3(111)$ STGB ($\phi = 70.5^\circ$) and stable $\Sigma 3(112)$ STGB ($\phi = 109.5^\circ$). Hydrogen trap energies of 0.49 eV are reported for the $\Sigma 3(111)$ STGB and 0.34 eV for the $\Sigma 3(112)$ STGB [35]. The non-ZPE-corrected value for the $\Sigma 3(111)$ STGB is 0.45 eV [36].

2.7 Free Surfaces

The hydrogen effect on the surface energy has long attracted interest because it is important in fracturing. The trap sites on the free surfaces, where hydrogen atoms are adsorbed, are classified according to the adsorption position, for example, onefold (1F), twofold (2F), threefold (3F), and fourfold (4F) sites. The hydrogen trap energies are summarized in Table 1. It is confirmed that the maximum hydrogen trap energy of the free surfaces is almost 0.75 eV and independent of the surface index.

2.8 Hydrogen Trap Energy of Trap Sites in Alpha Iron

The hydrogen trap energies of various trap sites in alpha iron are shown in Fig. 2. For reference, the hydrogen trap energies of various trap sites in aluminum are also shown in Fig. 3 [38]. It is quite interesting that when various trap sites are ordered

Table 1 Hydrogen trap energy of free surfaces [eV]

Adsorption site	{100} 4F	2F-1	{112} 2F-2	4F	{110} 3F	{111}
Trap energy	0.67 ^a	0.73 ^b	0.71 ^b	0.73 ^b	0.84 ^b	0.79 ^c

^aRef [37]

^bRef [14]

^cRef [36]

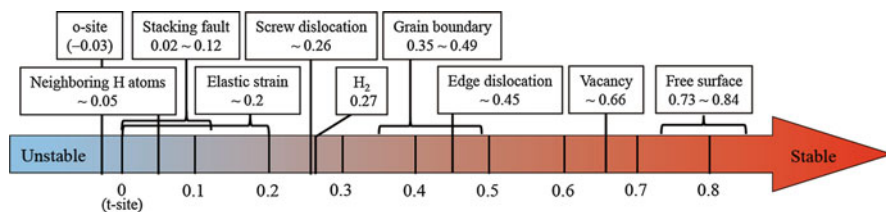


Fig. 2 Hydrogen trap energy of various trap sites in alpha iron [eV]

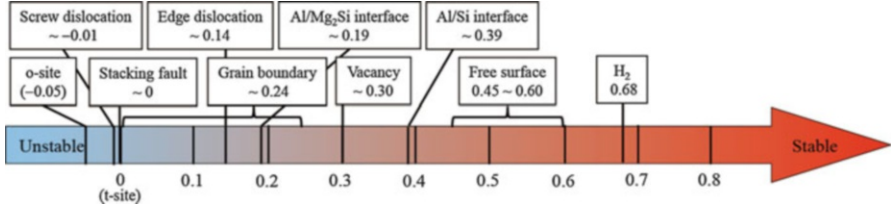


Fig. 3 Hydrogen trap energy of various trap sites in Al [eV]

according to the strength of the hydrogen trap energy, as shown in Figs. 2 and 3, the sequence is very similar even for different materials, i.e., free surface > vacancy > grain boundary > edge dislocation. Thus, it is suggested that there is a correlation between the local free volumes at trap sites and trap energy besides the chemical interaction with a third element. However, although the energy of the hydrogen molecule is most stable for aluminum, there is near screw dislocations in alpha iron. Thus, at thermal equilibrium, the hydrogen concentration in alpha iron is higher than in aluminum, and lattice defects in alpha iron trap more hydrogen atoms.

3 Hydrogen Effect on Individual Lattice Defects

3.1 Hydrogen Occupancy at Trap Sites

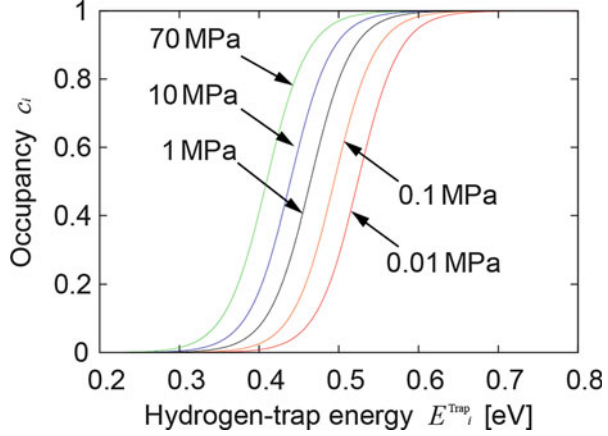
The basic steps of hydrogen embrittlement are believed to involve changes in the stability and mobility of lattice defects owing to the presence of hydrogen. Thus, capturing the fundamentals of the hydrogen effect on isolated lattice defects is important. To analyze the hydrogen effect on each lattice defect using atomistic and quantum-level simulations, allocating hydrogen atoms at stable sites with appropriate probability that corresponds to real conditions is essential. The procedure to evaluate the hydrogen occupancy at each trap site using the hydrogen trap energies, which were summarized in Sect. 2, is given. The relation at thermal equilibrium between hydrogen occupancy at a trap site with hydrogen trap energy E_i^{Trap} and hydrogen occupancy at the t-site in the undeformed lattice, c_i and $c_{t\text{-site}}$, respectively, is expressed as follows [39]:

$$\frac{c_i}{1 - c_i} = \frac{c_{t\text{-site}}}{1 - c_{t\text{-site}}} \exp\left(\frac{E_i^{\text{Trap}}}{k_B T}\right), \quad (2)$$

where k_B is the Boltzmann constant and T is the absolute temperature.

For hydrogen gas conditions of temperature T and pressure p , the $c_{t\text{-site}}$ is given by the following empirical relation [40]:

Fig. 4 Hydrogen occupancy vs. hydrogen trap energy for various hydrogen gas pressures at room temperature (300 K)



$$c_{t\text{-site}} = 0.9686 \times 10^{-6} \sqrt{p} \exp\left(-\frac{3440}{T}\right). \quad (3)$$

By defining p and T , the hydrogen occupancy at trap site c_i is calculated as a function of the trap energy E^{Trap}_i using Eqs. 1 and 2, as shown in Fig. 4. The hydrogen occupancy at lattice sites in metals can also be quantitatively evaluated under hydrogen atmosphere using first-principles calculations and lattice vibration analysis [41, 42] over a wide range of hydrogen conditions where experimental data are unavailable [43]. In this study, a similar relation between the hydrogen occupancy at the t-site and temperature and pressure, as shown in Eq. 3, is presented for alpha iron.

As shown in Fig. 4, c_i rapidly increases for $E^{\text{Trap}}_i > 0.4$ eV under various hydrogen gas pressures at room temperature. For example, at $T = 300$ K and $p = 70$ MPa, components exposed to high hydrogen gas pressures, such as pipes and tanks in fuel cell vehicles, $c_i > 0.5$ for $E^{\text{Trap}}_i > 0.41$ eV is obtained. Therefore, the free surfaces ($E^{\text{Trap}} \sim 0.75$ eV [14, 36, 37]) and vacancies ($E^{\text{Trap}} = \sim 0.65$ eV [26, 27]) trap hydrogen atoms with high probability at hydrogen gas conditions. The edge dislocation cores ($E^{\text{Trap}} \sim 0.44$ eV [16]) and high-energy GBs ($E^{\text{Trap}} = \sim 0.49$ eV [35]) also interact with hydrogen atoms. Conversely, the hydrogen concentrations around screw dislocation cores ($E^{\text{Trap}} < 0.30$ eV [32, 33]), low-energy GBs ($E^{\text{Trap}} \sim 0.34$ eV [35]), and stacking faults are relatively small.

Using computations, the lattice defects that trap hydrogen atoms are defined, and the distribution of hydrogen around each lattice defect is determined using random numbers and occupancy rates based on the distribution of the hydrogen trap energy around lattice defects. Thus, constructing atomistic models with realistic hydrogen distributions and concentrations for specific hydrogen gas pressures and temperature conditions is possible. Many theoretical calculations of hydrogen-lattice defect interactions have used extremely high hydrogen concentrations and artificial hydrogen distributions. In the following sections, the hydrogen effects on vacancies (Sect. 3.2), GBs (Sect. 3.3), and edge dislocations (Sect. 3.4) at practical hydrogen

concentrations are reviewed. These defects are related to the typical hydrogen embrittlement mechanisms, i.e., HESIV [11, 12], HEDE [5, 6], and HELP [7–10].

3.2 Hydrogen Effect on Vacancies

Using the hydrogen trap energy of a vacancy in Sect. 2.3 and the evaluation procedure of the hydrogen occupancy at each trap site in Sect. 3.1, we confirm that two hydrogen atoms are trapped by a vacancy under a wide range of hydrogen gas conditions. Matsumoto et al. estimated the apparent vacancy formation energy and the mobility of a vacancy when a vacancy traps two hydrogen atoms in hydrogen gas environment [27]. The apparent lattice defect energy is evaluated by the following equation:

$$W_f^{w-H} \approx W_f^{w/o-H} - \sum_i c_i (E_i^{\text{Trap}} + \mu_b), \quad (4)$$

where W_f^{w-H} and $W_f^{w/o-H}$ are the formation energy of the lattice defect with and without hydrogen, respectively. μ_b is the change in configurational entropy and is evaluated by the following equation:

$$\mu_b \approx k_B T \ln \left(\frac{c_{\text{t-site}}}{1 - c_{\text{t-site}}} \right). \quad (5)$$

At $T = 300$ [K] and $p = 70$ MPa, $c_{\text{t-site}} = 8.5 \times 10^{-8}$ and μ_b is -0.42 eV. Furthermore, using $W_f^{w/o-H} = 2.14$ eV, $E_1^{\text{Trap}} = 0.64$ eV, and $E_2^{\text{Trap}} = 0.66$ eV, W_f^{w-H} is estimated to be 1.68 eV. At thermal equilibrium, the concentration of vacancy is evaluated by the following equation:

$$C_0 = \exp \left(-\frac{W_f}{k_B T} \right). \quad (6)$$

The reduction in the vacancy formation energy from 2.14 to 1.68 eV owing to the presence of hydrogen increases the vacancy concentration from 1.12×10^{-36} to 6.00×10^{-29} . Although hydrogen increases seven orders of magnitude the vacancy concentration, the latter remains very low. Thus, the change in the vacancy concentration at thermal equilibrium does not affect the mechanical behavior of alpha iron.

The mobility of a vacancy is estimated by calculating the activation energy for migration using the climbing image nudged elastic band method [44, 45] and VASP [23–25]. The activation energy increases from 0.62 to 1.07 eV when a vacancy traps two hydrogen atoms. This change in the activation energy reduces the diffusion frequency from 1.71×10^2 to $6.42 \times 10^{-6} \text{ s}^{-1}$. Unlike the thermal equilibrium concentration of vacancy, the reduction in diffusion frequency may significantly affect the mechanical properties of alpha iron under hydrogen gas because the vacancy

diffusion is assumed to be zero and the vacancy concentration in a specific plane where many dislocation activities occur is supersaturated, as discussed in Sect. 4.3.

3.3 Hydrogen Effect on the Cohesive Energy of Grain Boundaries

It has been experimentally reported that the strength of materials in hydrogen environment improves by controlling the distribution of the misorientation angles of GBs [46]. The hydrogen effect on the GBs in alpha iron has been evaluated by using interatomic potentials [34] and first-principles calculations [35, 36, 47]. Yamaguchi and Gesari evaluated the hydrogen binding energy and cohesive energy of GBs using DFT calculations and demonstrated that hydrogen embrittles GBs [36, 47].

Matsumoto et al. [35] estimated the hydrogen concentration at GBs in alpha iron under hydrogen gas using DFT calculations and obtained the cohesive energy of GBs by assuming that the hydrogen atoms trapped in GBs are adsorbed on the halves on the generated two surfaces. From the DFT calculations, the reduction in cohesive energy was estimated to be approximately 25% for $\Sigma 3(111)$ STGB ($\phi = 70.5^\circ$) and almost zero for $\Sigma 3(112)$ STGB ($\phi = 109.5^\circ$). In contrast, Yamaguchi et al. revealed that the hydrogen effect is much pronounced when considering mobile hydrogen that diffuses to the surface during fracturing [48].

3.4 Hydrogen Effect on Dislocation Mobility

Dislocation movement is the fundamental process of plastic deformation. Therefore, it has attracted much attention with respect to the HE process and mechanism, e.g., HELP. Taketomi et al. reported that the Peierls potential for the $\{112\} \langle 111 \rangle$ edge dislocation is reduced in the presence of low hydrogen concentrations, 0.49/nm hydrogen atoms per unit length of dislocation line, i.e., approximately 300 K, 0.01 MPa hydrogen gas conditions from Sect. 3.1 [49]. Moreover, the interaction among neighboring dislocations, i.e., shear stress field, is almost the same even though the hydrogen concentration increases up to 7.35/nm [49]. To take into account the competition of dislocation movement and hydrogen diffusion, Taketomi et al. calculated the stress-dependent thermal activation energies for hydrogen diffusion and dislocation movement and estimated the dependence of the dislocation velocity on the applied shear stress [50]. The results demonstrated that the dislocation mobility increases (softening) with decreasing applied stress, whereas the dislocation mobility decreases (hardening) with moderate stress. For high applied stress, although the dislocation is pinned by hydrogen atoms at the beginning, the dislocation moves separately from hydrogen and does not interact during steady-state movement. Interestingly, stress-dependent softening or hardening only occurs at very low hydrogen concentrations. Taketomi et al. reported the hydrogen concentration effect on the Peierls potential [51], and the results suggested that only the hardening is dominant at high hydrogen concentration. Softening and hardening are also reported by Itakura et al. for screw dislocations using DFT calculations [31].

3.5 Interaction Between Hydrogen and Individual Lattice Defects

In this section, the procedure to evaluate the hydrogen occupancy at each trap site is first introduced. Then, it is shown that vacancies, grain boundaries, and edge dislocations can trap hydrogen atoms. Subsequently, the hydrogen effects on these lattice defects are reviewed.

4 Lattice Defects and Hydrogen Embrittlement Mechanisms

4.1 Interaction Between Many Lattice Defects

Experimentally observed hydrogen embrittlement results from the interaction among lattice defects during deformation and fracturing. In this section, we review the phenomena caused by the interaction among the hydrogen-affected lattice defects and the competition among the various microscopic mechanisms using large-scale MD and DD simulations, where the hydrogen effects on each individual lattice defect are modeled based on Sect. 3.

4.2 Cracks and Dislocations

The contrasting behavior for individual dislocation movements is suggested by the atomistic calculations, as reviewed in Sect. 3.4. However, plastic deformation is attributed to the multiple slips of numerous individual dislocations. In particular, the dislocations generated from a crack tip dominate the crack propagation and fracture process. Taketomi et al. performed simple discrete DD calculations around a mode-II crack tip [52] based on the results obtained by the atomistic calculations to evaluate the many-body effects of dislocations around a stress singularity of a crack tip. In that study, the effect of solute hydrogen on dislocation emission is also taken into account that hydrogen enhances the dislocation emission from a crack tip [53]. Thus, the multiple effects of hydrogen concentration and applied stress conditions affect the dislocation movement ahead of the crack tip. For low hydrogen concentrations ($C_H = 0.49/\text{nm}$ along the dislocation line), the dislocation slip region is extended under small applied stress intensity factor rate conditions comparable to the absence of solute hydrogen atoms. The slip region decreases with increasing applied stress rate; however, it does not show significant differences compared to the no hydrogen conditions. On the contrary, for the high hydrogen concentration case ($C_H = 1.24/\text{nm}$ along the dislocation line), the dislocation slip region is restricted near the crack tip owing to the hardening of the dislocation movement even when the solute hydrogen enhances the dislocation generation at the crack tip. The trend of dislocation localization is always realized for all ranges of applied stress intensity factor rate conditions. Considering the effects of hydrogen concentration and applied stress conditions on the dislocation movement, the elementary process of HE fracturing in an ideal material is summarized. The dislocation generation from a crack tip is the

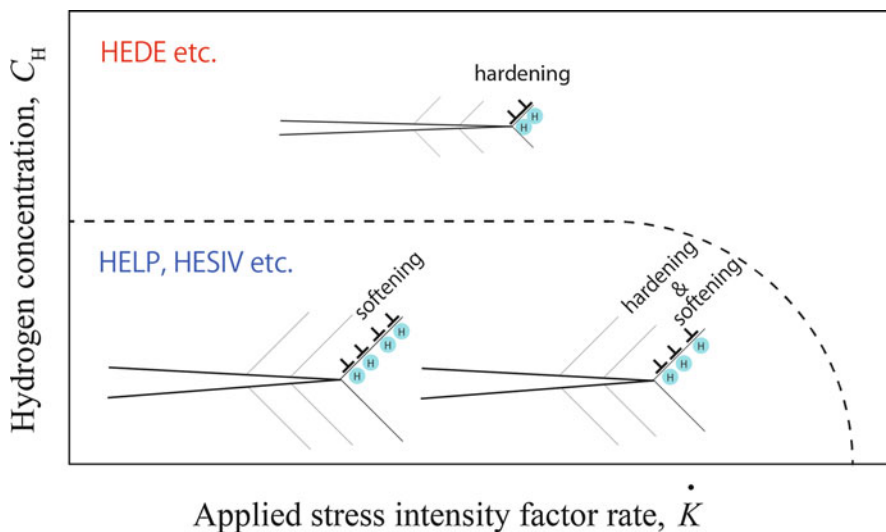


Fig. 5 Schematic of the transition of the HE fracturing mechanism for different hydrogen concentrations and applied stress intensity factor rate conditions for ideal materials

start of the plastic deformation and fracturing of a cracked ideal material. The dislocation slip behavior around a crack tip is enhanced at low hydrogen concentrations and low applied stress intensity factor rate conditions. The number of sliding dislocations increases in such conditions; thus, the plastic deformation around a crack tip increases and the fracture mechanism of HELP or HESIV would be dominant. The crack will blunt owing to the increased plastic deformation around a crack. At high hydrogen concentrations, in contrast, only hardening occurs independent of the applied stress intensity factor rate conditions. Therefore, the dislocation slip is restricted and the number of generated dislocations decreases. The crack shape becomes sharp and the hardening leads to brittle fracturing HEDE so far. The relations of the HE mechanisms for simplified ideal materials are shown in Fig. 5. The results strongly suggest that the HE mechanism changes depending on the combination of environmental and mechanical conditions even in the same material.

4.3 Supersaturation of Vacancy Concentration Associated with Plastic Deformation

Takai et al. showed that the vacancy concentration increases owing to plastic deformation under hydrogen conditions [54]. Jog dragging by a screw dislocation under shear stress was believed to be one of the mechanisms for the vacancy multiplication owing to plastic deformation. Matsumoto et al. estimated the vacancy distribution behind a jog, which is moving at constant velocity, using the hydrogen-affected physical properties of a vacancy obtained in Sect. 3.2 and the diffusion

equation [27, 55]. According to this report, although the vacancy distribution spreads behind the jog for the no hydrogen case, the vacancy does not show distinct diffusion and stays in the form of a line behind the jog even for slow dislocation velocity (10^{-8} m/s). The jog dragging of the screw dislocation is one of the examples for vacancy generation. This analysis suggests that supersaturated vacancies would locally accumulate during plastic deformation in HE.

4.4 Reduced Lattice Defect Energy (Defactant-Like Effects)

The complex interactions among the lattice defects and the effect of hydrogen atoms on them affect HE. MD simulations can model the complex interactions among the various lattice defects. The effects of hydrogen mostly become large at small deformation speeds because the hydrogen distribution follows the stress distribution at low deformation rates and responds to the defect nucleation and motion [56–58]. Hydrogen diffusion in materials is definitely extremely fast compared to the diffusion of other elements, and it is well known that the hydrogen distribution follows the movement of lattice defects and the stress distribution during deformation. Nevertheless, the diffusion is too slow to model by direct MD simulations.

Matsumoto et al. developed the interatomic potential with pseudohydrogen effects for alpha iron under hydrogen gas at 70 MPa and 300 K based on what is discussed in Sects. 2 and 3 [14] and analyzed the activity of many lattice defects and the interaction among them using large-scale MD simulations [59].

The interatomic potential incorporates the thermodynamic effects of hydrogen on the lattice defect energies, and thus, calculations of the hydrogen movement are not required. The kinetics of hydrogen and the time-dependent phenomena related to hydrogen diffusion are important in some cases; however, in this study, as a limiting case, the hydrogen-related phenomena appearing under equilibrium hydrogen distribution were examined.

MD simulations of (i) crack propagation, (ii) nanoindentation, and (iii) tensile loading of a polycrystalline nanorod are performed, and the effects of hydrogen on the deformation and fracturing under these boundary conditions are discussed. The results are also compared for the cases of with and without hydrogen using the Mendeleev potential for alpha iron [60]. The following conclusions were reached:

- (i) Crack growth simulations: The crack propagation behavior in alpha iron simulated with pseudohydrogen effects indicated that the material was extremely brittle, whereas crack propagation simulated without hydrogen effects occurred at a higher stress intensity factor after the emission of dislocations. This result corresponds to HEDE caused by the reduction in the surface energies.
- (ii) Nanoindentation: For the alpha iron simulated with pseudohydrogen effects, the pop-in load significantly decreased. Furthermore, dislocation loops were

generated toward the four bottom corners. These phenomena are occasionally referred to as HELP. In addition, as the indentation progressed, several vacancies were generated throughout the sample, which agrees with the HESIV mechanism.

- (iii) Tensile loading of a polycrystalline nanorod: For alpha iron simulated with pseudohydrogen effects, the sample ruptured along GBs in a brittle manner, whereas in the simulations without hydrogen effects, intergranular fractures did not occur, but a large amount of dislocation activity was observed. The intergranular fracturing occurred because hydrogen significantly reduces the cohesive energy of GBs when the maximum effects of hydrogen mobility are incorporated.

Although the MD simulation incorporated the hydrogen mobility effects through the interatomic potential with pseudohydrogen effects, it was shown that depending on the boundary conditions and initial material conditions, well-known hydrogen-related phenomena, i.e., HELP, HESIV, and HEDE, potentially appear despite the use of the same interatomic potential, i.e., same material system. Thus, the reduction in the defect formation energies leads to the well-known hydrogen-related phenomena, and the defactant-like effect of hydrogen plays a significant role in HE.

5 Summary, Future Directions, and Remaining Problems

In this chapter, recent studies that treat the HE of alpha iron from an atomistic viewpoint are reviewed. In Sect. 2, the hydrogen trap energies of various trap sites, i.e., elastic strain field, vacancy, edge and screw dislocations, stacking faults, grain boundaries, and free surfaces, in alpha iron are reviewed first. In Sect. 3, the hydrogen occupancy at each trap site under hydrogen gas conditions is first examined; then, the hydrogen effect on the vacancy, grain boundary, and edge dislocations that are lattice defects that trap considerable hydrogen atoms under such conditions is reviewed. In Sect. 4, the interaction among hydrogen-affected lattice defects and the competition among the various microscopic mechanisms are discussed. As shown in this chapter, the evaluation of the hydrogen concentration in defects under given boundary hydrogen concentrations is critical to the atomistic and quantum simulations. Moreover, the HE is strongly affected by environmental (hydrogen concentration) and mechanical (deformation rate, applied stress, stress concentration) conditions. Thereby, we note that HE varies depending on the conditions even in the same materials.

To fully understand hydrogen embrittlement, considering the competition of the various effects of hydrogen on lattice defects, including the time-dependent hydrogen diffusion, is critical. Lattice defects, which are dominant, are controlled by the boundary conditions, initial structure, and degree of deformation. Furthermore, the effect of added elements should also be clarified in a sequential manner.

References

1. Myers SM, Baskes MI, Birnbaum HK, Corbett JW, Deleo GG, Estreicher SK, Haller EE, Jena P, Johnson NM, Kirchheim R, Pearton SJ, Stavola MJ. Hydrogen interactions with defects in crystalline solids. *Rev Mod Phys*. 1992;64:559–617.
2. Birnbaum HK, Robertson IM, Sofronis P, Teter D. Mechanisms of hydrogen related fracture – a review. In: Magnin T, editor. *Corrosion Deformation Interactions CDI'96*, Nice; 1997. p. 172–195.
3. Lynch SP. Mechanisms of hydrogen assisted cracking – a review. In: Moody NR, Thompson AW, Ricker RE, Was GW, Hones RH, editors. *Hydrogen effects on materials behavior and corrosion deformation interactions*. Warrendale: TMS; 2003.
4. Nagumo M. *Fundamentals of hydrogen embrittlement*. Singapore: Springer; 2016.
5. Frohberg RP, Barnett WJ, Troiano AR. Delayed failure and hydrogen embrittlement in steel. *Trans ASM*. 1955;47:892–935.
6. Oriani RA, Josephic H. Equilibrium aspects of hydrogen induced cracking of steels. *Acta Metall*. 1974;22:1065–74.
7. Birnbaum HK, Sofronis P. Hydrogen-enhanced localized plasticity—a mechanism for hydrogen-related fracture. *Mater Sci Eng A*. 1994;176:191–202.
8. Ferreira PJ, Robertson IM, Birnbaum HK. Hydrogen effects on the interaction between dislocations. *Acta Mater*. 1998;46:1749–57.
9. Sofronis P, Robertson IM. Transmission electron microscopy observations and micro-mechanical continuum models for the effect of hydrogen on the mechanical behaviour of metals. *Phil Magazine A*. 2002;82:3405–13.
10. Murakami Y. The effect of hydrogen on fatigue properties of metals used for fuel cell system. *Int J Fract*. 2006;138:167–95.
11. Nagumo M, Nakamura M, Takai K. Hydrogen thermal desorption relevant to delayed-fracture susceptibility of high-strength steels. *Metall Mater Trans A*. 2001;32:339–47.
12. Monasterio PR, Lau TT, Yip S, Van Vliet KJ. Hydrogen-vacancy interactions in Fe-C alloys. *Phys Rev Lett*. 2009;103:085501.
13. Kirchheim R. On the solute-defect interaction in the framework of a defactant concept. *Int J Mater Res*. 2009;100:483–7.
14. Seki S, Matsumoto R, Inoue Y, Taketomi S, Miyazaki N. Development of EAM potential for Fe with pseudo-hydrogen effects and molecular dynamics simulation of hydrogen embrittlement. *J Soc Mater Sci Jpn*. 2012;61:175–82. (in Japanese)
15. Matsumoto R, Inoue Y, Taketomi S, Miyazaki N. Influence of shear strain on the hydrogen trapped in bcc-Fe: a first-principles-based study. *Scr Mater*. 2009;60:555–8.
16. Taketomi S, Matsumoto R, Miyazaki N. Atomistic study of hydrogen distribution and diffusion around a $\{112\} \langle 111 \rangle$ edge dislocation in alpha iron. *Acta Mater*. 2008;56:3761–9.
17. Sofronis P, Birnbaum HK. Mechanics of the hydrogen-dislocation-impurity interactions—I. Increasing shear modulus. *J Mech Phys Solid*. 1995;43:49–90.
18. Krom AHM, Bakker A, Koers RWJ. Modelling hydrogen-induced cracking in steel using a coupled diffusion stress finite element analysis. *Int J Pressure Vessels Piping*. 1997;72: 139–47.
19. Kotake H, Matsumoto R, Taketomi S, Miyazaki N. Transient hydrogen diffusion analyses coupled with crack-tip plasticity under cyclic loading. *Int J Pressure Vessels Piping*. 2008;85:540–9.
20. Takayama K, Matsumoto R, Taketomi S, Miyazaki N. Hydrogen diffusion analyses of a cracked steel pipe under internal pressure. *Int J Hydro Ene*. 2011;36:1037–45.
21. Cocharde AW, Schoek G, Wiedersich H. Interaction between dislocations and interstitial atoms in body-centered cubic metals. *Acta Metall*. 1955;3:533–7.
22. Clouet E, Garruchet S, Nguyen H, Perez M, Becquart CS. Dislocation interaction with C in α -Fe: a comparison between atomic simulations and elasticity theory. *Acta Mater*. 2008;56:3450–60.

23. Kresse G, Hafner J. Ab initio molecular-dynamics for open-shell transition-metals. *Phys Rev B*. 1993;48:13115–8.
24. Kresse G, Furthmüller J. Efficient iterative schemes for ab initio total-energy calculations using a plane-wave basis set. *Phys Rev B*. 1996;54:11169–86.
25. Kresse G, Furthmüller J. Efficiency of ab-initio total energy calculations for metals and semi-conductors using a plane-wave basis set. *Comput Mater Sci*. 1996;6:15–50.
26. Tateyama Y, Ohno T. Stability and clusterization of hydrogen-vacancy complexes in α -Fe: an ab initio study. *Phys Rev B*. 2003;67:174105.
27. Matsumoto R, Nishiguchi N, Taketomi S, Miyazaki N. First-principles calculation of hydrogen effects on the formation and diffusion of vacancies in alpha iron: discussion of the hydrogen-enhanced strain-induced vacancy mechanism. *J Soc Mater Sci Jpn*. 2014;63:182–7. (in Japanese)
28. Besenbacher F, Myers SM, Nordlander P, Nørskov JK. Multiple hydrogen occupancy of vacancies in Fe. *J Appl Phys*. 1987;61:1788–94.
29. Lu G, Zhang Q, Kioussis N, Kaxiras E. Hydrogen-enhanced local plasticity in aluminum: an ab initio study. *Phys Rev Lett*. 2001;87:095501.
30. Taketomi S, Matsumoto R, Miyazaki N. Atomistic study of hydrogen diffusion around dislocations in alpha iron. In: *Effects of Hydrogen on Materials. Proceedings of the 2008 International Hydrogen Conference, Jackson Lake; 2009*. p. 655–62.
31. Wen M, Xu XJ, Fukuyama S, Yokogawa K. Embedded-atom-method functions for body-centered-cubic iron. *J Mater Res*. 2001;16:3496–502.
32. Itakura M, Kaburaki H, Yamaguchi M, Okita T. The effect of hydrogen atoms on the screw dislocation mobility in bcc iron: a first-principles study. *Acta Mater*. 2013;61:6857–67.
33. Kimizuka H, Ogata S. Slow diffusion of hydrogen at a screw dislocation core in α -iron. *Phys Rev B*. 2011;84:024116.
34. Riku M, Matsumoto R, Taketomi S, Miyazaki N. Atomistic simulation study of cohesive energy of grain boundaries in alpha iron under gaseous hydrogen environment. *J Soc Mater Sci Jpn*. 2010;59:589–95. (in Japanese)
35. Matsumoto R, Riku M, Taketomi S, Miyazaki N. Hydrogen–grain boundary interaction in Fe, Fe–C, and Fe–N systems. *Prog Nucl Sci Tech*. 2010;2:9–15.
36. Yamaguchi M, Ebihara K, Itakura M, Kadoyoshi T, Suzudo T, Kaburaki H. First-principles study on the grain boundary embrittlement of metals by solute segregation: part II. Metal (Fe, Al, Cu)-hydrogen (H) systems. *Metall Mater Trans A*. 2011;42A:330–9.
37. Sorescu DC. First principles calculation of the adsorption and diffusion of hydrogen on Fe(100) surface and in the bulk. *Catal Today*. 2005;105(1):44–65.
38. Enomoto T, Matsumoto R, Taketomi S, Miyazaki N. First-principles estimation of hydrogen occupancy around lattice defects in al. *J Soc Mater Sci Jpn*. 2010;59:596–603. (in Japanese)
39. McLean D. *Grain boundaries in metals*. London: Oxford University Press; 1957.
40. Hirth JP. Effects of hydrogen on the properties of iron and steel. *Metall Trans A*. 1980;11:861–90.
41. Alfè D. PHON: a program to calculate phonons using the small displacement method. *Comp Phys Commun*. 2009;180:2622–33.
42. Togo A. Welcome – phonopy. Available from: <http://atztogo.github.io/phonopy/>. Accessed 26 Sept 2016
43. Matsumoto R, Sera M, Miyazaki N. Hydrogen concentration estimation in metals at finite temperature using first-principles calculations and vibrational analysis. *Comput Mater Sci*. 2014;91:211–22.
44. Vasp TST Tools. Available from: <http://theory.cm.utexas.edu/vtsttools/>. Accessed 27 Sept 2016
45. Henkelman G, Uberuaga BP, Jónsson H. A climbing image nudged elastic band method for finding saddle points and minimum energy paths. *J Chem Phys*. 2000;113:9901–4.
46. Bechtle S, Kumar M, Somerdar BP, Launey ME, Ritchie RO. Grain-boundary engineering markedly reduces susceptibility to intergranular hydrogen embrittlement in metallic materials. *Acta Mater*. 2009;57:4148–57.

47. Gesari S, Irigoyen B, Juan A. Segregation of H, C and B to $\Sigma=5$ (013) α -Fe grain boundary: a theoretical study. *Appl Surface Sci.* 2006;253:1939–45.
48. Yamaguchi M, Kameda J, Ebihara K, Itakura M, Kaburaki H. Mobile Effect of hydrogen on intergranular decohesion of iron: first principles calculations. *Philos Mag.* 2012;92:1349–69.
49. Taketomi S, Matsumoto R, Miyazaki N. Atomistic simulation of the effects of hydrogen on the mobility of edge dislocation in alpha iron. *J Mater Sci.* 2008;43:1166–9.
50. Taketomi S, Matsumoto R, Miyazaki N. Atomic study of the competitive relationship between edge dislocation motion and hydrogen diffusion in alpha iron. *J Mater Res.* 2011;26:1269–78.
51. Taketomi S, Matsumoto R, Miyazaki N. Molecular statics study of the effect of hydrogen on edge dislocation motion in alpha-Fe. In: Somerday BP, Sofronis P, editors. *Hydrogen-materials interactions: ASME, 2 Park Avenue, New York, NY 10016, USA; 2014.* p. 765–70.
52. Taketomi S, Imanishi H, Matsumoto R, Miyazaki N. Dislocation dynamics analysis of hydrogen embrittlement in alpha iron based on atomistic investigations. In: *Proceedings of 13th International Conference Fracture, ICF13, Beijing; 2013.* p. 5721–9.
53. Taketomi S, Matsumoto R, Miyazaki N. Atomistic study of the effect of hydrogen on dislocation emission from a mode II crack tip in alpha iron. *Int J Mech Sci.* 2010;52:334–8.
54. Takai K, Shoda H, Suzuki H, Nagumo M. Lattice defects dominating hydrogen-related failure of metals. *Acta Mater.* 2008;56:5158–67.
55. Karthikeyan S. Evaluation of the jogged-screw model of creep in equiaxed gamma-TiAl: identification of the key substructural parameters. *Acta Mater.* 2004;52:2577–89.
56. Kotake H, Matsumoto R, Taketomi S, Miyazaki N. Transient hydrogen diffusion analyses coupled with crack-tip plasticity under cyclic loading. *Int J Press Vess Pip.* 2008;85:540–9.
57. Doshida T, Nakamura M, Saito H, Sawada T, Takai K. Hydrogen-enhanced lattice defect formation and hydrogen embrittlement of cyclically prestressed tempered martensitic steel. *Acta Mater.* 2014;61:7755–66.
58. Matsuoka S, Tanaka H, Homma N, Murakami Y. Influence of hydrogen and frequency on fatigue crack growth behavior of Cr-Mo steel. *Int J Fract.* 2011;168:101–12.
59. Matsumoto R, Seki S, Taketomi S, Miyazaki N. Hydrogen-related phenomena due to decreases in lattice defect energies—molecular dynamics simulations using the embedded atom method potential with pseudo-hydrogen effects. *Comput Mater Sci.* 2014;92:362–71.
60. Mendelev MI, Han S, Srolovitz DJ, Ackland GJ, Sun DY, Asta M. Development of new interatomic potentials appropriate for crystalline and liquid iron. *Philos Mag.* 2003;83:3977–94.